Surface layer Chl*a* concentrations, as derived from ocean color remote sensing, have long functioned as a central property for monitoring global changes in marine phytoplankton. Variability and trends in Chl*a* reflect both adjustments in phytoplankton biomass and physiology (or health). Both of these properties are mechanistically linked to physical properties of the upper ocean, as well as ecological relationships between phytoplankton and their zooplankton predators. Unraveling this diversity and often covariation of factors that influence Chl*a* concentrations is essential for correctly interpreting the implications of Chl*a* anomalies for ocean biogeochemistry and food webs. For example, inverse relationships between Chl*a* and SST can emerge from changes in either mixed-layer light levels or vertical nutrient flux, but these two mechanisms have opposite implications for phytoplankton NPP (Behrenfeld et al. 2016). An additional complication is that measured changes in ocean color often reflect, at least in part, changes in colored dissolved organic matter signals (Siegel et al. 2005) that are mistakenly attributed to Chl*a* changes (Siegel et al. 2013). Thus, while the satellite record of ocean color continues to provide critical insights on global processes, new insights and approaches are needed to fully understand the story these data are telling regarding relationships between climate and marine ecosystems.

j. Global ocean carbon cycle—R. A. Feely, R. Wanninkhof, P. Landschützer, B. R. Carter, and J. A. Triñanes

The global ocean is a major sink for anthropogenic carbon dioxide (CO_2) that is released into the atmosphere from fossil fuel combustion, cement production, and land use changes. Over the last decade the global ocean has continued to take up a substantial fraction of the anthropogenic carbon (C_{anth}) emissions and is therefore a major mediator of global climate change. Of the 10.2 ($\pm$0.7) Pg C yr^{-1} C_{anth} released during the period 2006–15, about 2.6 ($\pm$0.5) Pg C yr^{-1} (26%) accumulated in the ocean, 3.1 ($\pm$0.8) Pg C yr^{-1} (30%) accumulated on land, and 4.5 ($\pm$0.1) Pg C yr^{-1} (43%) remained in the atmosphere (Global Carbon Project 2016). This decadal ocean carbon uptake estimate is a consensus view based on a combination of measured decadal inventory changes, models, and global air–sea CO_2 flux estimates based on surface ocean partial pressure of CO_2 (pCO_2) measurements. Using ocean general circulation models that include biogeochemical parameterizations (OBGCMs) and inverse models that are validated with observations-based air–sea exchange fluxes and basin-scale ocean inventories, Le Quéré et al. (2016) have demonstrated

that the oceanic anthropogenic carbon sink has grown from 1.2 ($\pm$0.5) Pg C yr^{-1} in the decade of the 1960s to 2.6 ($\pm$0.5) Pg C yr^{-1} in the decade from 2006 to 2015. Air–sea flux studies reported here indicate an ocean uptake of C_{anth} of 2.5 ($\pm$0.5) Pg C yr^{-1} for 2016, with the uncertainty being the standard deviation of monthly values.

1) Air–sea carbon dioxide fluxes

Ocean uptake of C_{anth} can be estimated from the net air–sea CO_2 flux derived from the bulk flux formula with air–sea differences in CO_2 partial pressure (ΔpCO_2) and gas transfer coefficients as input (Wanninkhof 2014). A steady contribution of carbon from continental runoff estimated at 0.45 Pg C yr^{-1} (Jacobson et al. 2007) is included to obtain the C_{anth}. The data source for pCO_2 are annual updates of surface water pCO_2 observations from the Surface Ocean CO_2 Atlas (SOCAT) composed of mooring and ship-based observations (Bakker et al. 2016). The ΔpCO_2 and a parameterization of the gas transfer with wind described in Wanninkhof (2014) are used to calculate the air–sea CO_2 fluxes. Increased observations and improved mapping techniques (e.g., Rödenbeck et al. 2015) now afford global pCO2 fields at a 1° grid on monthly time scales with a lag of less than three months. This progress allows investigation of variability on subannual to decadal time scales.

The monthly 2016 ΔpCO_2 maps are based on an observation-based neural network approach (Landschützer et al. 2013, 2014) applied to biogeographical provinces. Surface temperature, sea surface salinity, climatological mixed-layer depth, satellite chlorophyll-a, and atmospheric CO_2 are used to establish relationships with surface ocean pCO_2 measurements and are applied where no observations exist. The 2016 air–sea estimate uses wind speeds from 2015 as consistent global wind products for 2016 have not been processed. Changes in winds over time have a small effect on gas transfer (Wanninkhof and Triñanes 2017) so this approximation should not have a determining impact on the interpretation of the air–sea CO_2 fluxes calculated for 2016.

The C_{anth} fluxes from 1982 to 2016 (Fig. 3.27) suggest a decreasing ocean sink in the first part of the record and a strong increase from 2001 onward. The amplitude of seasonal variability is ~1 Pg C with minimum uptake in June–September. The C_{anth} air–sea flux of 2.5 ($\pm$0.5) Pg C yr^{-1} in 2016 is 32% above the 2005–14 average of 1.9 ($\pm$0.5) Pg C yr^{-1}.

The average fluxes in 2016 (Fig. 3.28a) show the characteristic pattern of effluxes in the tropical regions, with the largest effluxes in the equatorial Pa-
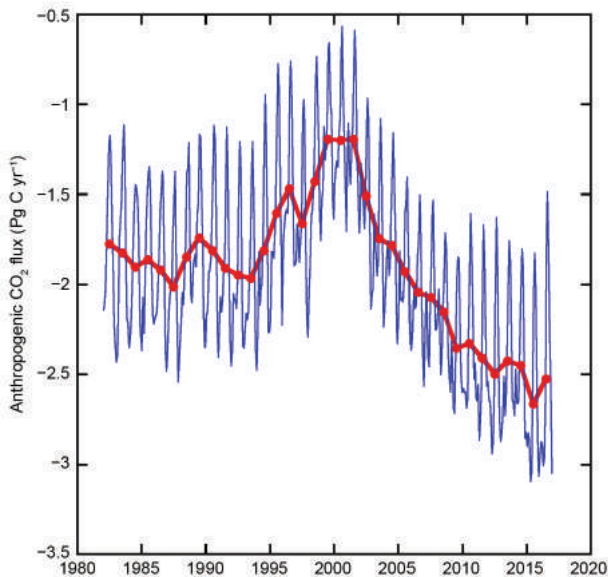
Fig. 3.27. Annual (red line) and monthly (blue line) C_{anth} fluxes (Pg C yr^{-1}) from 1982–2016. Negative values indicate uptake by the ocean.

cific and Arabian Sea upwelling regions. Large sinks are observed poleward of the subtropical fronts. The Southern Ocean is a strong sink but net annual effluxes are apparent in the Polar Front regions (55°–60°S) in the Indian and Pacific sectors of the Southern Ocean.

Ocean uptake anomalies (Fig. 3.28b) in 2016 relative to the 1995–2015 average are attributed to the increasing ocean CO_2 uptake with time and to several climate reorganizations. The air–sea flux trend since 2000 is −0.7 (±0.08) Pg C decade^{-1}, which leads to predominantly negative flux anomalies (greater uptake). Despite this strong trend there are several regions showing positive anomalies for 2016, notably the eastern equatorial, western, and North Pacific. The subtropical gyres in the North Atlantic and southern Indian Oceans show positive anomalies as well. The positive anomalies are attributed to changes in ocean circulation patterns; however, they are often difficult to attribute to a single cause. The increased effluxes in the eastern equatorial Pacific are possibly caused by the changes in ENSO patterns, with the largest impacts of the recent El Niños being farther west in the central rather than eastern equatorial Pacific (Ashok and Yamagata 2009). Stronger effluxes in the western and North Pacific are related to strongly positive PDO values in 2015–16 as well as the residual of the 2013–15 warm anomaly in the northern North Pacific (Bond et al. 2015) that persisted into the first half of 2016 (Fig. 3.28c).

The differences between the air–sea CO_2 fluxes in 2016 compared to 2015 (Fig. 3.28c) are easier to place in context of changes in temperature, circulation, and

climate reorganizations as the longer-term trends do not obfuscate the changes. The anomalously high CO_2 effluxes in the northeast Pacific associated with the anomalously warm temperatures of the 2013–15 warm anomaly have shifted northward in this region. The equatorial Pacific shows an increase in CO_2 fluxes near the equator associated with increasing upwelling after the termination of the 2015/16 El Niño. This shift is also reflected by cooler SST in the region (see Fig. 3.1). The strong increase in uptake in the Atlantic subpolar gyre in 2016 is associated with warmer SST, suggesting that less cold deep waters with high pCO_2 were entrained into the surface mixed layer. The strong positive flux anomaly near the polar front in the southeastern sector of the South Pacific Ocean is likely associated with regionally enhanced upwelling of cold deep water with high CO_2. This
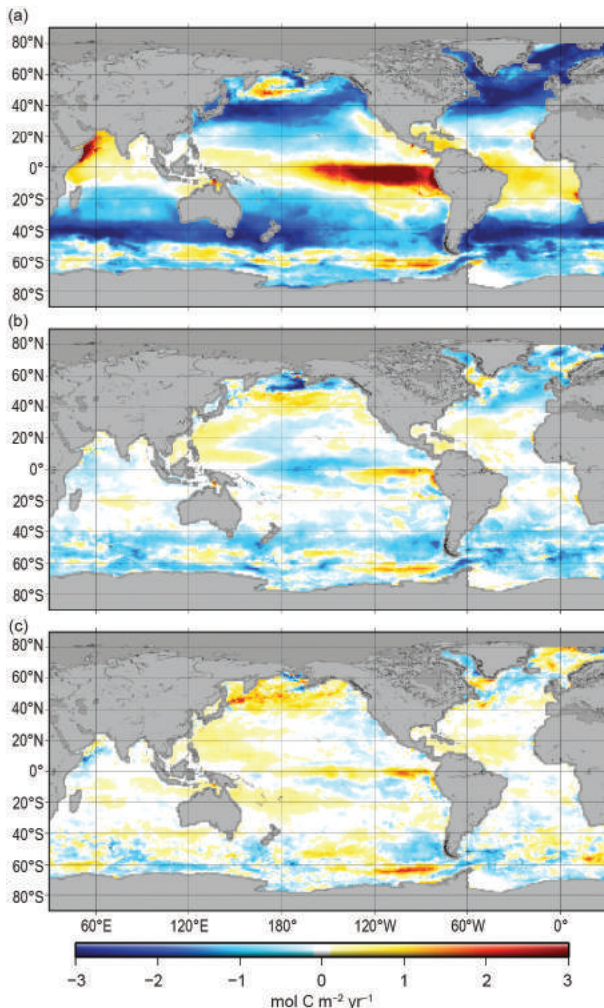

Fig. 3.28. (a) Net air–sea fluxes for 2016; **(b)** net air–sea flux anomalies for 2016 compared to the average for 1995–2015; and **(c)** net air–sea flux anomalies for 2016 compared to the 2015 values following the method of Landschützer et al. (2013). Anomalies are in mol C m^{-2} yr^{-1}.

feature has the expected small negative SST anomaly associated with it. However, the SST anomaly appears greater in the Atlantic sector and has a strong negative, rather than a positive, flux anomaly associated with it. This relation shows that, while many of the flux/pCO_2 anomalies can be attributed to climate reorganizations and associated physical anomalies, notably temperature, the causality is often complex. For example, the behavior of pCO_2 with respect to temperature includes competing processes: thermodynamics dictate decreasing pCO_2 with decreasing SST but waters originating from the deep with a cold temperature signal will have a high pCO_2.

The strong trend of increasing uptake since 2002 reached its largest uptake value in 2015 and in 2016 has decreased slightly, largely to decreased uptake in June–September (Fig. 3.27). This small decrease in global uptake is well within the envelope of interannual variability and should not be inferred as a longer-term saturation of the ocean CO_2 sink.

2) Carbon inventories

The U.S. Global Ocean Ship-based Hydrographic Investigations Program (GO-SHIP) is providing new information about the uptake and storage of carbon within the ocean interior by determining the change in measured dissolved inorganic carbon (DIC) concentrations and calculations of estimated C_{anth} concentration changes between decadal cruise reoccupations. A recent example is the DIC concentrations (Figs. 3.29a,c,e) and the DIC differences (Figs. 3.29b,d,f) for the three P18 cruises that occurred in 2016/17, 2007/08, and 1994. The high decadal DIC differences among the P18 cruises in the Pacific show the buildup of DIC of up to 50 µmol kg^{-1} resulting from gas exchange, mixing, and transport of the water masses in the surface and intermediate waters to depths down to approximately 1500–2000 m. On these approximately decadal time scales, increases are expected in the lighter density thermocline waters found shallower than ~2000 m. These increases are owing to continued surface ocean uptake of CO_2, which are in turn owing to atmospheric increases caused by human activities, primarily burning of fossil fuels. Apparent noise in this increase is due to large
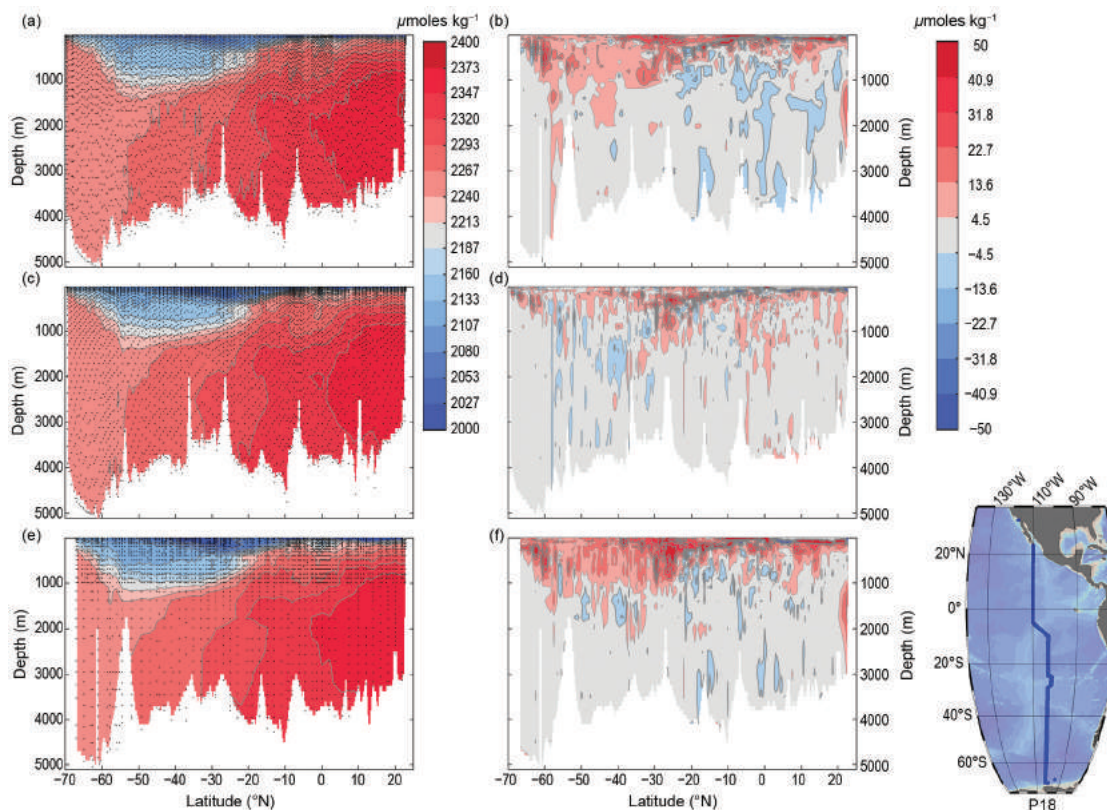
FIG. 3.29. Vertical-meridional sections of total DIC measured along the GO-SHIP P18 section in (a) 2016/17, (c) 2007/08, and (e) 1994. DIC change sections (red indicates increases) between (b) 2007/08 and 1994 cruises, (d) 2016/17 and 2007/08 cruises, and (f) 2016/17 and 1994 cruises. For this comparison, measured property values were interpolated vertically using a cubic Hermite piece-wise polynomial method and interpolated linearly against latitude onto a fixed grid.

DIC variability from changes in ocean circulation on decadal and shorter time scales. Planned future work will quantify the fraction of the observed changes that are directly attributable to increases of CO_2 from human activities. These increases are expected to propagate into deeper waters on longer time scales.

Using a modified version of the extended multiple linear regression (eMLR) method with Pacific cruise data, Carter et al. (2017) determined that the Pacific Ocean (from 60°N to 60°S) accumulated an average of 6.1 (±1.6) Pg C decade^{-1} in the decade of 1994–2004 as compared with 8.9 (±2.2) Pg C decade^{-1} during the decade of 2004–14 (Table 3.3). The eMLR approach uses linear regressions to determine the empirical relationships between properties of interest and other hydrographic properties (salinity, potential temperature, nitrate, and silicic acid) that are also affected by water mass movements but not affected by increases in C_{anth}. The difference between the regression constants from the earlier and later datasets are then used to estimate the changes in ocean carbon independent of any changes in the water mass distributions. Using a similar approach for the Atlantic, Woosley et al. (2016) showed that C_{anth} storage increased from 5.1 to 8.1 Pg C decade^{-1} over the same time intervals. These results suggest that both increases in air–sea exchange of CO_2 at the surface as well as changes in ventilation within the ocean interior contribute to increased rates of uptake in the later decade. Because of the vast area of the subtropical gyres, the majority of the C_{anth} inventory is stored in the subtropics. By contrast, upwelling regions near the equator, in the North Pacific, and in the Southern Ocean south of the Antarctic Circumpolar Current have low storage rates (Table 3.3). In these regions, upwelling of deep waters that have been isolated from the atmosphere since the preindustrial era displace the better-ventilated, higher C_{anth} intermediate depth waters. Anthropogenic carbon inventories inferred from these different approaches are consistent with each other. (Available online at www.nodc.noaa.gov/OC5/woa13.)

TABLE 3.3. Pacific decadal C_{anth} storage for the latitude bands in Pg C decade^{-1}. The "total" values include estimates for data-poor latitude bands from 60° to 67°N and 70° to 80°S, and therefore do not exactly equal the sum of all rows (after Carter et al. 2017).

Latitude Band	WOCE to CLIVAR	CLIVAR to GOSHIP
70°–60°S	†	0.65
60°–50°S	0.56	0.84
50°–40°S	0.90	0.97
40°–30°S	0.96	1.07
30°–20°S	0.65	1.31
20°–10°S	0.35	1.20
10°–0°S	0.29	0.72
0°–10°N	0.46	0.56
10°–20°N	0.79	0.52
20°–30°N	0.60	0.64
30°–40°N	0.35	0.53
40°–50°N	0.13	0.35
50°–60°N	0.07	0.21
Southern Hemisphere	3.8 ± 1.0	6.8 ± 1.7
Northern Hemisphere	2.4 ± 0.6	2.8 ± 0.7
Total (60°S–60°N)	6.1 ± 1.6	8.9 ± 2.2
† insufficient data		